7

Laser-induced Fluorescence Spectroscopy

Laser-induced fluorescence (LIF) is (spontaneous) emission from atoms or molecules that have been excited by (laser) radiation. The phenomenon of induced fluorescence was first seen and discussed back in 1905 by R. W. Wood, many decades before the invention of the laser. The process is illustrated schematically in Figure 7.1.

If a particle resonantly absorbs a photon from the laser beam, the particle is left in an excited energy state. Such a state is unstable and will decay spontaneously, emitting a photon again. As has been discussed earlier, the excited state of finite lifetime emits its photon on return to a lower energy level in random directions. It is this fact that allows one to measure an absorption signal directly, as outlined in Chapter 6. Conveniently, the fluorescence is observed at 90° to a collimated laser beam. In principle, a very small focal volume V_c may be defined in the imaging set-up, resulting in spatial resolution of the laser–particle interaction volume; note that spatial resolution cannot normally be realized in an experiment, which measures the absorption directly.

In a sense, the method of LIF may be seen as a fancy way of measuring the absorption of a species, but with a bonus. Absorption spectroscopy, which detects the transmitted light, has (in many experimental implementations) a limited sensitivity. The problem is that one has to detect a minute amount of missing light in the transmitted beam, i.e. one encounters the problem of the difference of large near-equal numbers. The use of pulsed lasers aggravates the problem due to their normally substantial pulse-to-pulse intensity fluctuations, which limit the signal-to-noise ratio. With fluorescence detection the signal can be detected above a background, which is (at least in favourable cases) nearly equal to zero, and detection at the single-photon level is relatively easy to achieve.

As is obvious from the above picture, two radiative transitions are involved in the LIF process. First, absorption takes place, followed by a second photon-emission step. Therefore, when planning a LIF experiment one should always bear in mind that LIF requires considerations associated with absorption spectroscopy. Any fancy detection equipment is merely used to detect the consequences of the absorption, with the additional information on how much was absorbed where.

One major caveat with fluorescence measurements is that they are no longer associated with a simple absolute measure of the absorbed amount of radiation (and therewith particle concentration). Too many difficult-to-determine or outright unknown factors influence the observed signal. Amongst these factors are spectroscopic quantities, such as quenching, and experimental quantities, such as observation angle and optics transmission, to mention

Laser Chemistry: Spectroscopy, Dynamics and Applications Helmut H. Telle, Angel González Ureña & Robert J. Donovan
 ISBN: 978-0-471-48570-4 (HB) ISBN: 978-0-471-48571-1 (PB)

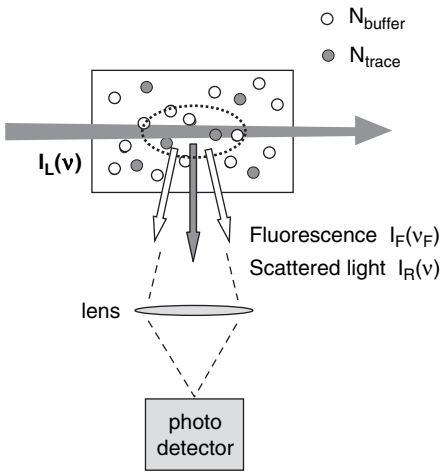

Figure 7.1 Principle of fluorescence emission, $I_F(\nu_F)$, from particles in a gas mixture, after absorption of tuneable laser light $I_L(\nu)$. Scattered light $I_R(\nu)$ at the same frequency as the incoming laser light is also observed

just a few. Of course, one can describe the fluorescence spectral emission quantitatively provided one knows or can estimate both spectroscopic and experimental parameters that influence it (see Box 7.1).

Despite this analytical shortcoming, its extreme sensitivity accounts for the popularity of LIF in many fields, including the investigation of chemical processes, and for many decades LIF has been one of the dominant laser spectroscopic techniques in the probing of unimolecular and bimolecular chemical reactions.

7.1 Principles of laser-induced fluorescence spectroscopy

In their simplest form, the processes involved in a LIF experiment are summarized in Figure 7.2 for a simple two-level model particle.

If the particle is resonantly stimulated by the laser source, then a photon of energy $h\nu_{12}$ will be absorbed, lifting the particle to the excited state. As is well known, both stimulated and spontaneous emissions have to be considered in the temporal decay of the excited level, where the relative ratio between the two is determined by the laser intensity. It should be noted that the stimulated emission process constitutes a loss mechanism for LIF observation at right angles, as

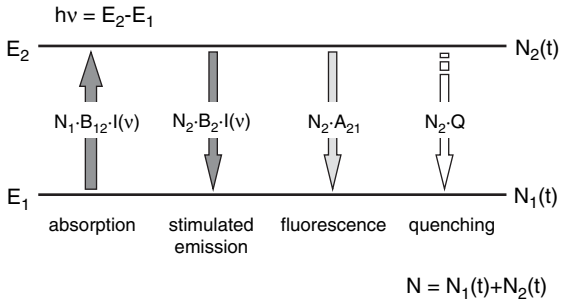

Figure 7.2 Radiative and non-radiative processes in a two-level system

shown in Figure 7.1, because those photons propagate in the direction of the incoming laser beam. A further loss to the signal to be observed is related to collisional quenching of the excited energy level, without the emission of a photon. Although quenching may not be a problem in high-vacuum conditions, where the time between collisions is normally much longer than the radiative lifetime, many experiments are run under conditions in which collisional quenching is important; this will be discussed further in some of the examples given below.

It also should be noted that scattered light at the same wavelength as the excitation light may obscure a fluorescence signal if the latter is also observed on the same downward transition wavelength as the excitation. However, with suitably fast detection electronics one can distinguish between the two: scattering occurs instantaneously, whereas the duration of the fluorescence signal depends on the lifetime of the upper energy level.

As the species looked at in chemical reactions are mostly molecules, the two electronic levels depicted in Figure 7.2 split into sub-levels, according to the molecular vibrational and rotational energy quanta. The vibrational levels are customarily numbered with the quantum number $v_i (i = 0, 1, 2,...)$. The notation for the rotational levels is more complex and depends as well on the size of the molecule, but typically one associates the rotation with the quantum number $J_i (i = 0, 1, 2,...)$. In order to distinguish between states, double primes are used to mark the (lower) ground-state levels and single-primed quantum numbers mark the excited (upper) state levels. The main processes observed in molecule–laser photon interactions are shown in Figure 7.3.

The absorption starts at a distinct rotational and vibrational level within the lower electronic (ground)

Box 7.1

Quantification of laser-induced fluorescence signals

The fluorescence spectral radiant power $\Phi_F(\nu)$ that an optical system will collect from the laser interaction volume to a detector is, to a good approximation, given by

$$\Phi_F(\nu) = \varepsilon h\nu A_{21} \frac{\Omega_c}{4\pi} \int_{V_c} n_2 F(\nu)\, dV_c \tag{7.B1}$$

where ε is the efficiency of the collection optics (including losses due to internal absorption and reflection at optical interfaces), h is Planck's constant, ν is the optical frequency of the transition, A_{21} is the Einstein coefficient for spontaneous emission (which is the probability of decay in any direction), $\Omega_c/4\pi$ is the fractional solid angle seen by the collection optics, n_2 is the population density of the excited state under laser excitation, and $F(\nu)$ is the normalized line shape function, which describes the spectral distribution of the emitted fluorescence. The integral is over the focal volume V_c, defined by the intersection of the laser beam and the collection optics.

The total fluorescence radiant energy Q_F arriving at the detector (with light frequency dispersion capability, if required) will be

$$Q_F = \int_{\Delta t} \int_{\Delta \nu_{det}} \Phi_F(\nu)\, d\nu\, dt \tag{7.B2}$$

The integration is over the spectral interval response interval of the detector and over a suitable time interval, associated with the duration of the laser excitation and the actual fluorescence lifetime.

Most likely n_2 will be a function of time, and thus combining Equations (7.B1) and (7.B2) and taking into account this time dependence yields

$$\begin{aligned} Q_F &= \varepsilon h\nu A_{21} \frac{\Omega_c}{4\pi} \int_{V_c} \int_{\Delta t} \int_{\Delta \nu_{det}} n_2(t) F(\nu)\, d\nu\, dt\, dV_c \\ &= \underbrace{\varepsilon h\nu A_{21} \frac{\Omega_c}{4\pi} \int_{V_c} \int_{\Delta \nu_{det}} F(\nu)\, d\nu\, dV_c}_{C} \int_{\Delta t} n_2(t)\, dt \\ &= C \int_{\Delta t} n_2(t)\, dt \end{aligned} \tag{7.B3}$$

C is defined as a calibration 'constant' that incorporates all geometrical (time-independent) constants and variables; this constant can, in general, be calculated to a reasonable precision, although ancillary measurements may be required to come to grips with the evaluation of the effective interaction volume (e.g. particle densities and the laser intensity are rarely uniform across the observation volume).

In Figure 7.3, the fluorescence process for a multi-level molecule is illustrated. In the scheme shown in Figure 7.3, the laser is tuned to one absorption transition. Fluorescence decay is then observed to all lower lying levels that can be reached via allowed transitions. In addition, collisions may populate levels adjacent to the excited state; thus, fluorescence from those secondary excited states will be observed as well. If the fluorescence is spectrally resolved, then each individual transition can be observed, and the result is called the *fluorescence spectrum*. If several different transitions are excited in sequence and the total fluorescence signal observed in each case, then the result is called the *excitation spectrum*. In any case, the total fluorescence energy collected from each transition is always of the form given by Equation (7.B2).

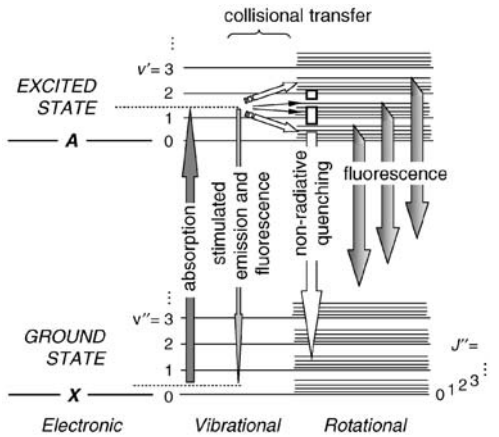

Figure 7.3 Radiative (absorption, stimulated emission, fluorescence) and non-radiative (quenching, collisional energy transfer, elastic scattering) processes in a molecular system with electronic, vibrational and rotational energy levels

state of the species under investigation and leads to a distinct level within an electronically excited state. The energy difference between the two levels is associated with the energy of the incident photon. Emission from the excited quantum state is possible to all lower lying energy levels, to which transitions are allowed, governed by the quantum selection rules for electronic dipole transitions (see Chapter 2). By and large one finds a multitude of emission lines; their intensities may be measured globally (integration of the whole light intensity) or individually. Both methods provide useful information, as will be discussed in Section 7.2.

In addition to the non-radiative quenching mentioned further above, an addition collisional energy transfer process can be observed, namely the transfer from the laser-excited level to neighbouring quantum levels within the excited-state manifold. Hence, under the right conditions, one observes lines from levels that were not directly populated by the laser excitation.

It is quite clear from the simplified schematic in Figure 7.3, and the associated discussion, that the selection of suitable excitation lines and the interpretation of LIF spectra can be an art. Figure 7.4 shows an example for absorption (lower part) and emission (upper part) spectra of the same molecular transition band, namely the $(X, 0'') \leftrightarrow (A, 0')$ band system of the OH radical generated in the photolysis of water.

Clearly, the discrete energies, i.e. discrete wavelengths corresponding to a molecular excitation and emission, coincide exactly with each other. Additional lines are noticeable in the emission spectrum, indicating transitions between different state manifolds as a consequence of collisional energy transfer in the excited state.

Although the absorption spectrum exhibits a large number of wavelengths at which the molecule could be excited, one of the main issues in the design of an LIF experiment is (to stress this again) the question of which line is the most suitable: the strongest line may not necessarily be the best. Of course, strong absorption is desirable, since it leads to a strong fluorescence; on the other hand, strong absorption may have to be avoided in order for the laser beam to reach the interaction region or the fluorescence leaving it. Both are attenuated in the passage through a column of absorbers; thus, a compromise has to be found between strong initial absorption and efficient emission light collection. Of course, if the density of particles in the system is very low, then this problem diminishes; however, in many practical cases of chemical reaction probing it is an issue.

Detectability limits and dynamic range constraints are often set by the nature of the chemical kinetics involved, and in which type of environment the measurements are carried out. Clearly, many (radical) species as the end result of a chemical reaction may only have vanishingly small concentrations. For those studying the specific kinetics of a reaction, these small concentrations are certainly of interest, since they provide insight into the

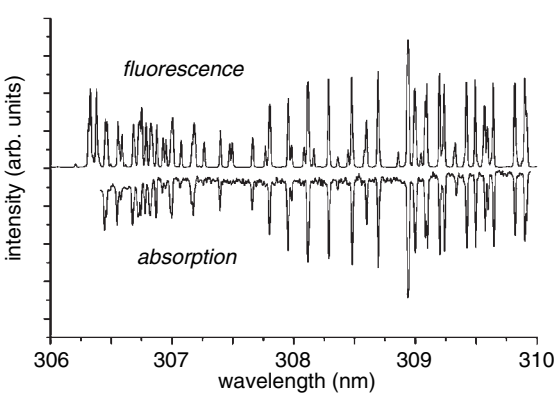

Figure 7.4 Comparison of absorption and LIF spectra for OH(X–A; $\Delta v = 0$); the OH radical was generated by photolysis of H_2O

global picture of branching into reaction channels. However, from a practical point of view (e.g. in an industrial production process) there is usually some limit below which the concentration of a species is insignificant with regard to the overall process. On the other hand, if one includes the detection of hazardous compounds in the environment as an object of study by LIF, then the range of concentrations over which measurement is desirable may be indeed extremely small, down to concentrations of parts per trillion (ppt).

7.2 Important parameters in laser-induced fluorescence

The overall aim in the investigation of reaction dynamics of chemical processes is to obtain a detailed picture of the path (or paths) that links reactants to products in a chemical reaction, as will be discussed in great detail in Parts 4 and 5. The 'dynamics' of a reaction can be characterized by measurements of some or all of the following important aspects (not a complete list):

- *Reagent properties*. In which way is the reaction influenced by properties such as reagent quantum state, velocity or light polarization (which induces spatial orientation of the particle in resonance with the radiation)?

- *Product quantum state*. Does one observe recognizable deviations from a thermal level population distribution (both vibration and rotation)?

- *Product velocity distribution*. Is the collision energy channelled into product translation and/or internal excitation?

- *Product angular distribution*. Are the observed products 'scattered' forwards, backwards or isotropically?

- *Product lifetimes*. Does the reaction proceed through a complex intermediate, and/or is the product affected by predissociation?

These questions may be addressed if reactions are studied with product state resolution, under single collision conditions (i.e. products are detected before they can undergo secondary collisions, so that their motion is characteristic of the forces experienced during the reaction). Then one can often work backwards from the measured product parameters to infer the processes that must have occurred during the reactive collision. Thus, one gains insight into the forces and energetics governing the reaction, associated with the particular potential energy surfaces (PESs) for the reaction. Some of these parameters and their measurement, and what can be learned from the data, are described in more detail below.

Product quantum state information derived from laser-induced fluorescence measurements

The LIF signal can be used in a number of ways. Most simply, it provides a measure of the population of the excited state (or states) through Equation (7.B3) deduced in Box 7.1. In addition, if a relationship can be found between the number densities of all quantum states involved in the excitation–emission sequence, then the total number density of the species can be deduced. However, a further wealth of information can be extracted from the LIF signals. As pointed out above, there are two basic approaches to the recording of LIF spectra. In the first, one excites the species under investigation in a single quantum transition and records the emission utilizing a wavelength-selective detection system, commonly known as the *fluorescence spectrum*. In the second, one tunes the exciting laser across all transitions accessible within its spectral range and records the fluorescence globally (integrated over all emission wavelengths); the result is known as the *excitation spectrum*.

An example for a fluorescence spectrum is shown in Figure 7.5 for the molecule CH_2O; note the strong signal at the wavelength of the laser excitation line, which amplifies the argument that, in order to eliminate the contribution of scattered light to the LIF spectrum, observation conveniently should be done at a wavelength different from the excitation. Fortunately, because of the vibrational–rotational energy-level manifolds encountered in molecules, this can mostly be realized.

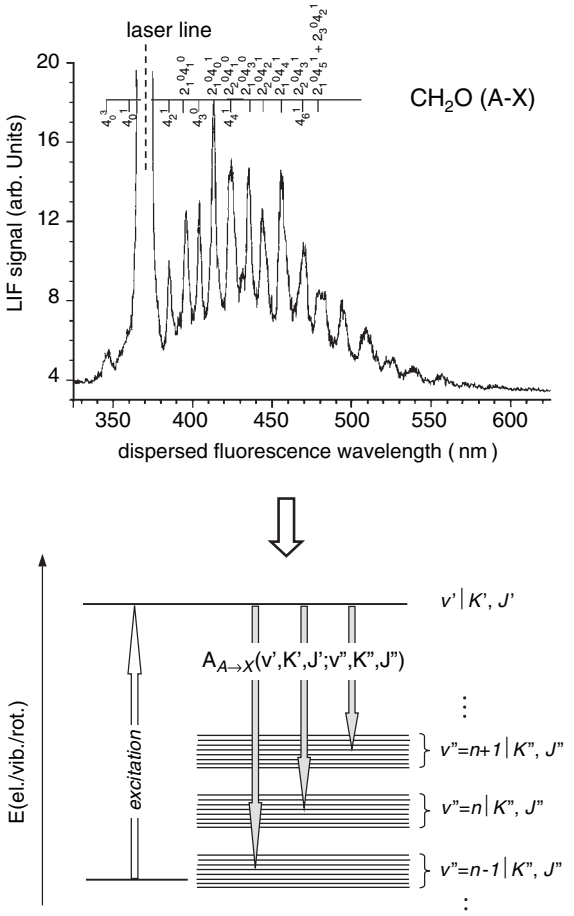

Figure 7.5 Dispersed fluorescence spectrum of formaldehyde (CH_2O) following laser excitation of its $X-A$ 4_1^0K(2) R(6) transition. Information on the energy-level structure and transition probabilities can be extracted from the line positions and the line intensities. Experimental data adapted from Klein-Duwel *et al*; *Appl. Opt.*, 2000, **39**: 3712, with permission of the Optical Society of America

The spectrum in Figure 7.5 reveals a sequence of (vibrational) bands, with resolution of rotational transitions in favourable cases. The energy-level structure can be deduced from the positions of the emission lines in the spectrum. In tuning the excitation laser sequentially to a number of different excited states, one can build up the complete vibrational–rotational energy-level manifold of the ground state.

In addition to the energy-level structure deduced from the fluorescence line positions, one can also derive information related to transition probabilities. In particular, one exploits that the overall transition probability expression for molecular transitions can be factorized into electronic, vibrational and rotational contributions (see Equation (2.4) in Section 2.2).

By scanning the probe laser over one or more rotational branches of the product, the relative intensities of the lines in this excitation spectrum may be used to determine product rotational (and/or vibrational) state distributions. In order to arrive at fully quantitative answers, corrections have to be made for relative transition probabilities, fluorescence lifetimes of the excited state, and any wavelength-dependent detection functions (such as the detection system spectral response). But once this has been done, one can deduce the ground state distribution function(s) by examining the so-called *excitation spectrum* of a molecular species. For thermal equilibrium conditions, the level population N_i can be described using a Boltzmann distribution function with temperature as the most important parameter; in its most general form this is

$$N_i(v,J) = (N_0/Z)g_i \exp(-E_i/kT) \qquad (7.1)$$

where ν and J are respectively the vibrational and rotational quantum level numbers; N_0 is the total number of particles in the ensemble; Z is a normalization factor, the so-called partition function, which guarantees that $\Sigma N_i(v,J) = N_0$; g_i is the statistical weight factor, which depends on rotational and vibrational state properties; E_i is the total quantum energy of a particular level; k is the Boltzmann constant; and T is the temperature.

The overall population distribution function can be factorized into their rotational and vibrational contributions according to

$$\begin{aligned} N(J) &= (2J+1)\exp(-E_{\text{rot}}/kT_{\text{rot}}) \quad \text{and} \\ N(v) &= g_v \exp(-E_{\text{vib}}/kT_{\text{vib}}) \end{aligned} \qquad (7.2)$$

These functions exhibit the well-known appearance of a bell-type function, tailing off towards higher rotational quantum numbers for rotation and an exponential decrease with increasing vibrational quantum number.

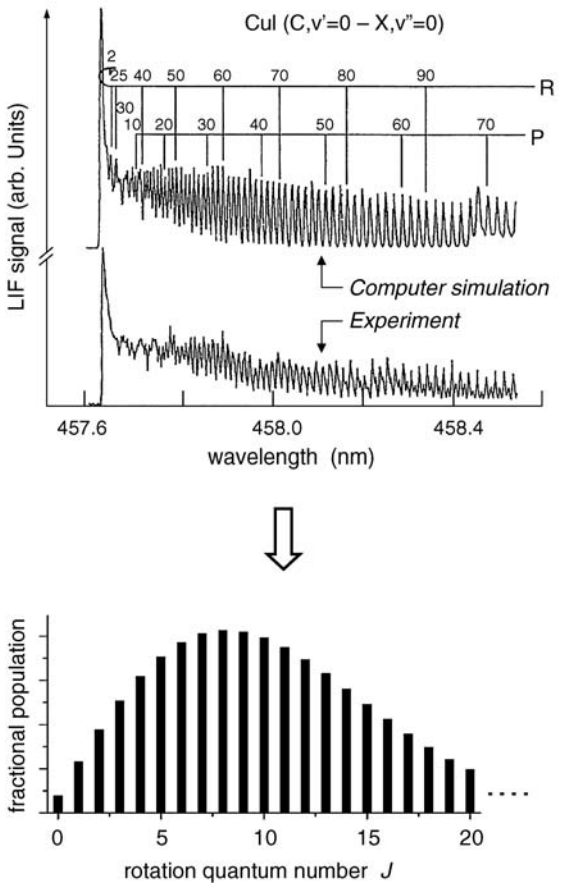

Figure 7.6 LIF excitation spectrum for the CuI(C, $\nu' = 0$–X, $\nu'' = 0$) band, with rotational line resolution, originating from the molecular beam reaction $Cu + I_2 \rightarrow CuI + I$. Level population information can be extracted from the spectral intensities (bottom). Experimental data adapted from Fang and Parson, *J. Chem. Phys.*, 1991, **95:** 6413, with permission of the American Institute of Physics

An example for the principle of extracting a distribution function from an LIF spectrum is shown in Figure 7.6.

It should be noted that the observed distribution functions might not be thermal. In fact, for a large number of product state distributions from uni- and bi-molecular reactions, one observes significant deviations form the Boltzmann functions, which reflect particular state-to-state chemical reaction dynamics.

It should also be noted that, with knowledge of the results from LIF experiments, which provide the energy-level structure and population information in a particular molecular state, one is able to simulate electronic transitions and their ro-vibrational bands from the derived spectroscopic parameters. An example for this procedure is shown in Figure 7.7; here, the simulated spectrum of the SrF(X–B) transition bands matches the observations extremely well, even reproducing the undulating feature of rotational state interference, when they coincide, or not, at the same wavelength position.

Study of individual laser-induced fluorescence transition lines

In general, the species under observation, the excitation system, and the detection system all have different line widths associated with them. Normally, one finds that $\Delta\nu_{\text{det}} \gg \Delta\nu_{\text{mol}}$, $\Delta\nu_{\text{las}}$ for the related widths parameters. The relative relation between the latter two depends very much on whether the laser is a pulsed laser or a CW laser; the half-width of a nanosecond-duration pulsed laser is normally much larger than the Doppler profile of the atom or molecule, whereas the opposite holds for CW lasers.

Thus, using a narrow-bandwidth laser, in addition to quantum-state-resolved measurements of the product, one can access the velocity and angular momentum distributions by making detailed measurements on a single rotational transition line. The transition is scanned at high resolution to resolve the Doppler line shape, effectively providing a 1D projection of the particle velocity along the probe laser propagation direction. Ultimately, by repeating such a measurement in different geometries, full 3 D spatial velocity distributions could be derived. This could be done both for reagents and for products in a chemical reaction.

For example, by measuring the Doppler profile in the direction of an atomic or molecular beam, and perpendicular to it, one can determine the translational energy contribution to a reaction. An example for such a measurement is shown in Figure 7.8. Clearly, the average velocity in the propagation direction of the beam is much larger than the distribution in the perpendicular coordinate; from the longitudinal velocity component, the kinetic energy

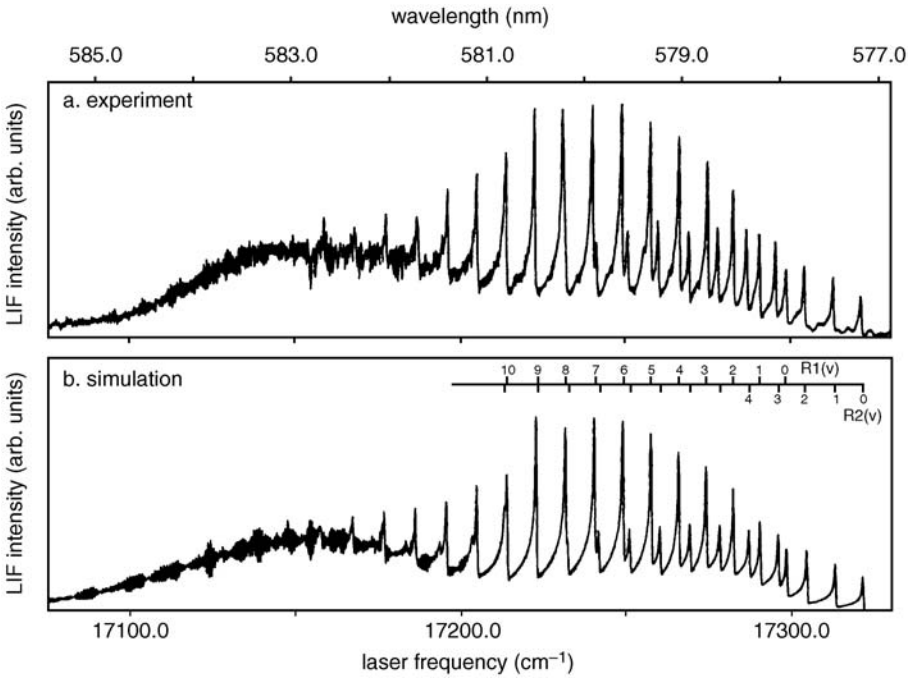

Figure 7.7 Experimental (a) and calculated (b) LIF spectra of SrF(B–X; $\Delta v = 0$), formed in the reaction $Sr^*(^3P_1) + HF$, for spectral resolution of 0.4 cm^{-1}. The wiggle-like structure seen at the long-wavelength side is due to partially resolved rotational lines in the tail of the R-branches. Reproduced form Teule *et al*; *J. Chem. Phys*., 1998, **102:** 9482, with permission of the American Institute of Physics

$E_{kin} = \frac{1}{2}mv^2$ in a subsequent reactive collision can be derived.

A similar velocity-measuring experiment can be carried out, for example, for product molecules. But, instead of physically altering the propagation direction of the laser beam, one may exploit that different experimental geometries are also defined by the relative orientation of the laser propagation plus its polarization directions, and the particle movement. A sufficient number of related one-dimensional velocity projections allow for the reconstruction of a full 3 D velocity distribution. Information on angular momentum alignment can also be extracted because the transition probability depends on the relative orientation of the laser polarization and the total angular momentum vector of the probed product. An example for this type of 3 D velocity profile reconstruction is shown in Figure 7.9 for the example of OH generated as a product in the reaction $H + N_2O \rightarrow OH + NO$ (Brouard *et al*., 2002). In this particular example, the results allowed the researchers to conclude from the stereodynamic reconstruction that the OH product was back scattered and that the reaction proceeded via a complex intermediate.

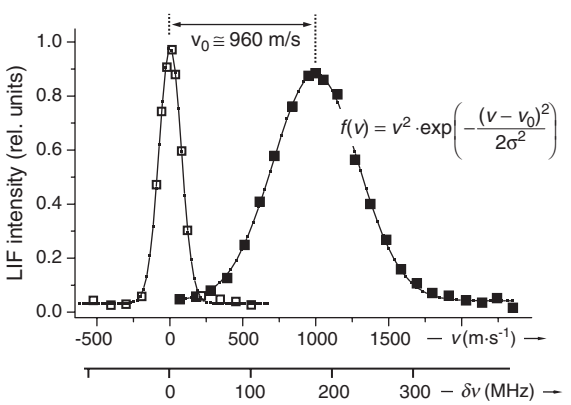

Figure 7.8 Transverse and longitudinal velocity distribution of Ca atomic beam, derived from the LIF response induced by a narrow-bandwidth CW dye laser ($\Delta\nu_L \approx$ 5 MHz)

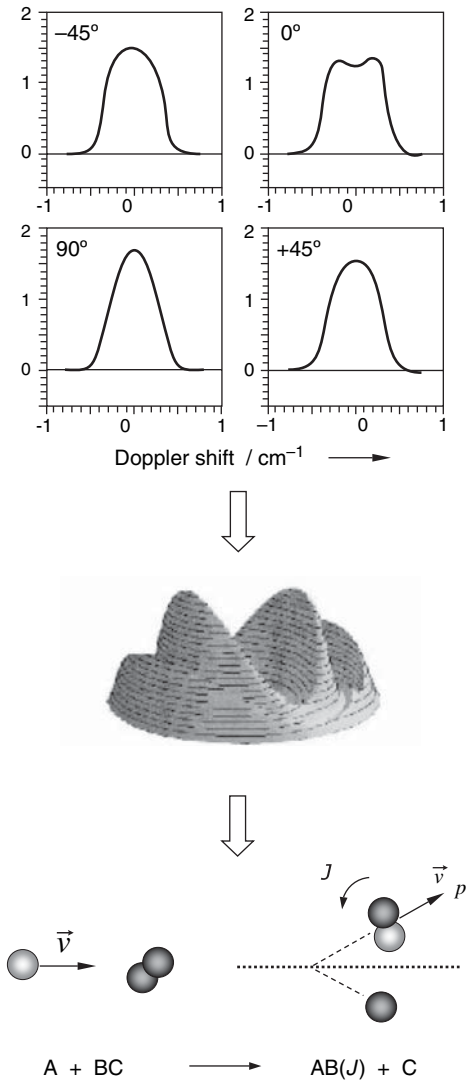

Figure 7.9 Raw experimental Doppler profile LIF data of the product state OH(X; $v' = 0, J' = 5$), for different laser light polarization directions (clockwise from top $-45°, 0°, 45°, 90°$), which are converted into 3D velocity–angle polar plots of the product scattering distribution. Information on the reaction stereodynamics can be extracted from the data. Experimental data adapted with permission from Brouard *et al, J. Phys. Chem. A* **106:** 3629. Copyright 2002 American Chemical Society

Pressure and temporal aspects in laser-induced fluorescence emission

In order to realize easily observable products from chemical reactions, the number density of reagents and subsequent products needs to be sufficiently high so that laser spectroscopic techniques generate measurable signals. However, with increasing number density, or gas pressure, secondary effects beyond that of the original reaction are observed. Specifically, in LIF experiments, the excited-state lifetime can become longer than the average time between collisions. This will influence this fluorescing state, resulting in apparent shortening of the lifetime, broadening of the transition line profile, and reduction in the LIF signal amplitude. Although this is frequently seen as an annoying effect in an LIF experiment, it may actually be used to derive important parameters of the reaction itself or about the interaction of a particular molecular state with its environment. Thus, experiments are often designed to follow the collisional effects as a function of gas pressure.

When the particle density is sufficiently small that on average radiative decay after excitation occurs well before a secondary collision, it should be possible, to directly measure the natural lifetime of the excited molecular (or atomic) energy level, $\tau = (\Sigma A_{ij})^{-1}$, as outlined in Chapter 2. The goal of any data analysis of time-resolved fluorescence is to extract the excited-state lifetime(s) from the excitation $I_0(t)$ and emission data $I_F(t)$. Normally, the two are not independent of each other and the relation of the actually observed fluorescence signal to the pure radiative decay would have to be calculated from the rate equations of the photon–particle interaction. However, if the fluorescence lifetime is longer than the overall duration of the excitation pulse, then the evolution of the level population, and hence the fluorescence signal, follows the simple spontaneous decay equation for the excited state once the excitation laser pulse is over. Thus, plotting the fluorescence intensity, on a logarithmic scale, against time will result in apparent linear dependence, and the lifetime is calculated from the slope of the resulting line (see Figure 7.10a).

If, on the other hand, the fluorescence lifetime is shorter than or of the same order as the excitation pulse, then the decay must be deconvolved from the excitation pulse, because the overall fluorescence signal response is represented, to a good approximation by

$$I_L \otimes I_F \propto \int I_L(t - t_0) n_i(t) \exp(-t/\tau)\, dt \qquad (7.3)$$

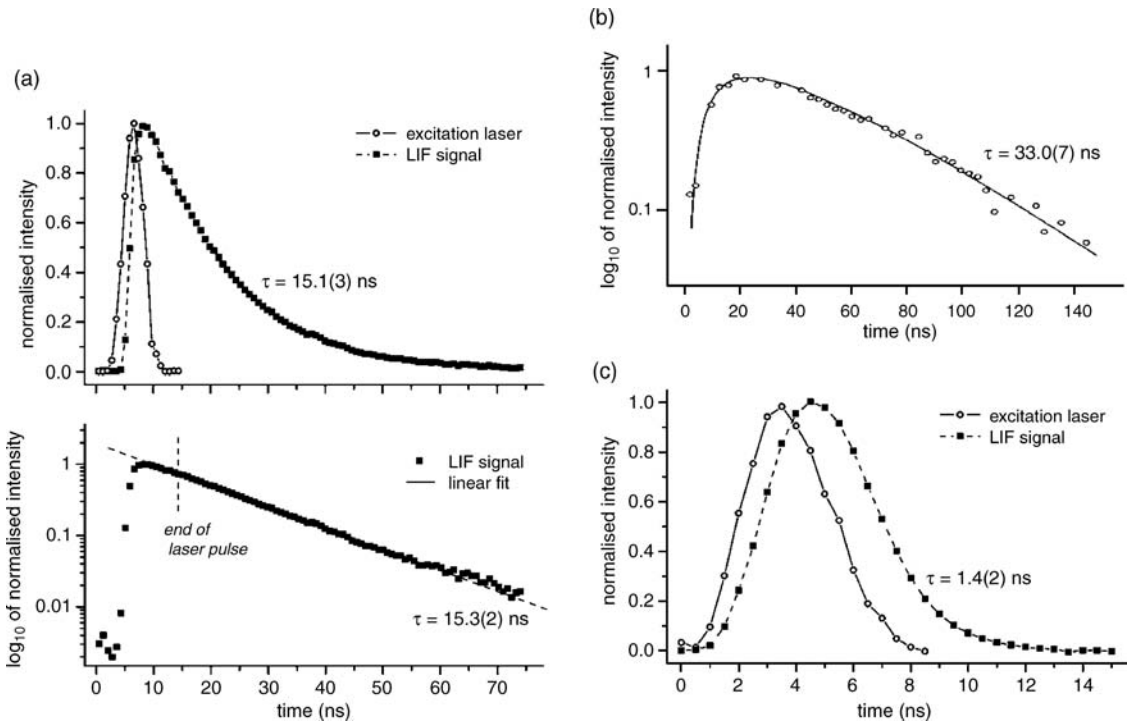

Figure 7.10 LIF lifetime measurements, following an excitation laser pulse of duration $\Delta\tau \cong 4.5$ ns FWHM. If the lifetime of the excited level is longer than the excitation pulse, then the lifetime can be extracted from the slope of the semi-logarithmic plot (trace a); if the radiative lifetime signal is detected with electronics of similar time constants, then *RC*-response deconvolution needs to be applied (trace b); and if the lifetime is of similar length or slightly shorter than the laser pulse, full line shape function deconvolution procedures are required (trace c). Data shown in trace (b) are adapted from Verdasco *et al*; *Laser Chem.*, 1990, **10**: 239, with permission of Taylor & Francis Group

where t_0 is the time when the laser pulse commences (or any other convenient time reference), and $\otimes$ represents the convolution operator. A common algorithm for retrieving the lifetime in this case is the method of least-squares iterative re-convolution: the (known) excitation pulse is convolved with an exponential decay function of varying lifetime parameter until that parameter most closely matches the emission data (see Figure 7.10b).

As soon as collisions start to occur on a scale comparable to the radiative lifetime, the evolution of the upper state population is affected. The lifetime of a transition is apparently shortened. This shortening can be associated with the rate of quenching collisions and one arrives at an effective lifetime equation

$$\tau_{\text{eff}}^{-1} = \tau^{-1} + k_{\text{Q}}(p, T) + k_{\text{D}} \qquad (7.4)$$

where $k_{\text{Q}}(p, T)$ (s^{-1}) is the quenching rate, which depends on the pressure and temperature of the collision gas. Note that the quenching rate is often expressed in the form $k_{\text{Q}} = k_{\text{q}}p$, where k_{q} ($\text{cm}^3\,\text{s}^{-1}$) is the pressure-independent quenching coefficient and p (cm^{-3}) is the pressure expressed in terms of the particle number density. The final factor, k_{D}, is associated with a possible predissociation rate for particular energy levels (see further below). An example of how the measurement of the collision-affected lifetime can result in useful information is shown in Figure 7.11.

First, from plotting the fluorescence lifetime data in the form τ_{eff}^{-1} versus pressure, one can extract the natural radiative lifetime. This is useful in cases for which no collision-free environment can be realized. Second, from the slope of the plot one can extract the quenching rate constant k_{Q}, which in itself is associated with the quenching cross-section of the

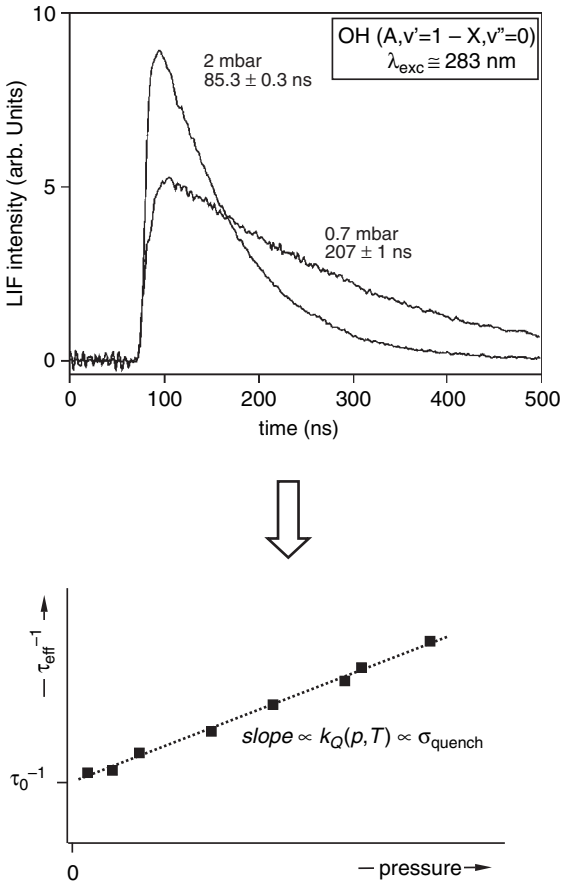

Figure 7.11 LIF signal decay of OH(A, $v' = 1$), after excitation from (X, $v'' = 0$) at $\lambda \cong 283$ nm, as a function of time. Information on the quenching cross-section can be extracted from the measured effective life times for different pressures. Note that $\tau_{\text{eff}}^{-1} = \tau^{-1} + k_{\text{Q}}(p, T) + k_{\text{P}}$, with $\tau^{-1} = A_{ji}$ the spontaneous emission rate, $k_{\text{Q}}(p, T)$ is the collisional quenching rate, and k_{P} is the predissociation rate

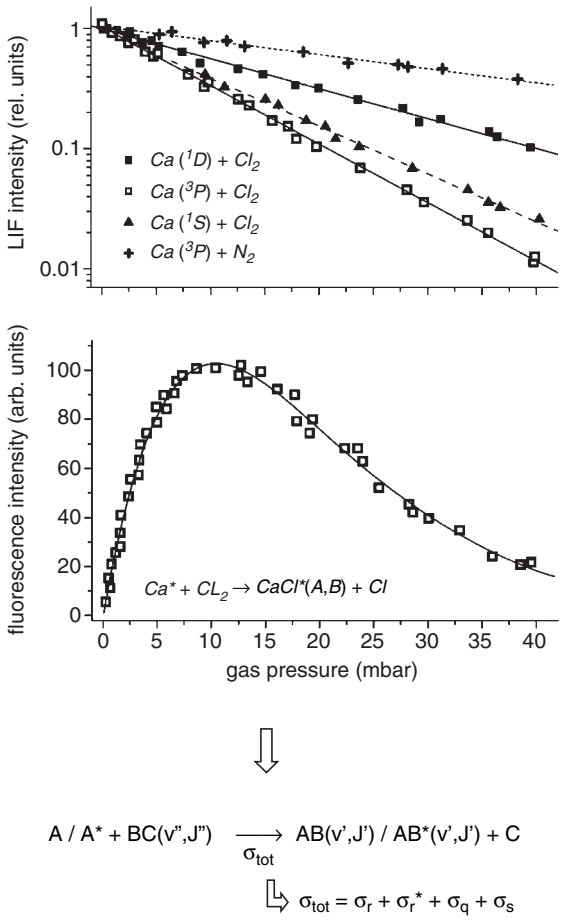

Figure 7.12 LIF probing of the reagent atom and simultaneous measurement of the total product fluorescence in the reaction $Ca/Ca^{*} + Cl_2 \rightarrow CaCl\,(X, A, B) + Cl$, as a function of (reactive) gas pressure. Information on total and reactive cross-sections can be extracted from the data (σ_{r} and σ_{r}^{*}: reaction cross-sections into ground and excited products; σ_{Q}: quenching cross-section; σ_{S}: elastic scattering cross-section)

collision σ_{quench}; both parameters are commonly used in the description of chemical reaction processes. It should be noted that, in general, one will be unable to conclude from a simple plot like the one in Figure 7.11 whether the quenching of the excited-state population is due to non-radiative deactivation or a consequence of a chemical reaction; additional measurements are normally required.

Such additional measurements can, for example, take the form of the data shown in Figure 7.12. A set of LIF intensity data for a beam–gas reaction is plotted against gas pressure in the chemical reaction (and probe) volume for the specific case of the reactive collision

$$\text{Ca}(^1\text{S}_0, ^3\text{P}_J, ^1\text{D}_2) + \text{Cl}_2 \rightarrow \text{CaCl}(\text{X}, \text{A}, \text{B}) + \text{Cl}$$

In addition to the LIF-attenuation data for the Ca reagent atom in its various excitation levels, data for the yield of the reactive channel into electronically

excited products, $Ca^*(A, B)$, were monitored via their chemiluminescence emission; and for the 'dark' channel, CaCl(X) LIF excitation spectra were recorded (not shown). By combining information from all data plots, the individual components of the total quenching cross-section

$$\sigma_{tot} = \sigma_r + \sigma_r^* + \sigma_Q + \sigma_S$$

can be extracted. Here, σ_r and σ_r^* are the reaction cross-sections into ground- and excited-state products, σ_Q is the non-radiative quenching cross-section, and σ_S is the (elastic and/or inelastic) scattering cross-section. The latter can be measured by probing for the presence of reagent and product states outside the interaction volume, or by the appearance of fluorescence from energy levels that were not directly populated by the laser excitation. For comparison, attenuation data for the non-reactive collision $Ca^* + N_2$ are included, which clearly underpin the notion that the other collisions are indeed efficiently yielding reaction products.

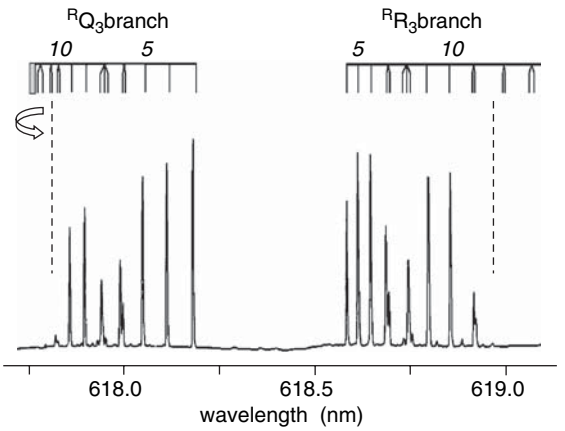

Figure 7.13 LIF spectrum of HNO for the $v = 100$–000 K = 4–3 sub-band of the $\tilde{X}^1A'' - \tilde{A}^1A'$ transition. The band clearly breaks off above $J' = 11$, marked by the dashed lines. Data adapted from Pearson *et al, J. Chem. Phys.*, 1997, **106**: 5850, with permission of the American Institute of Physics

Predissociation probed by laser-induced fluorescence

The final topic addressed in this section is that of predissociation of molecules. It is the interaction between energy level configurations, which initiate the transfer from one (chemically stable) state to another (chemically unstable) state. The difference with respect to photon interaction promoting the molecule from a lower to a higher energy level is that the predissociation interaction is a molecule-internal quantum process. Predissociation after an excitation can be detected in a number of ways, e.g. including the appearance of a daughter product or the unexpected disappearance (cut-off) of lines in a rotational/vibrational band sequence. The latter is normally easy to recognize and it does not require any additional probe experiment to be conduced. An example is shown in Figure 7.13 in the LIF excitation spectrum for a sub-band in HNO ($\tilde{X} \rightarrow \tilde{A}$); clearly, the break-off of the rotational band beyond the quantum level $J' = 11$ in the $\tilde{A}$ state is observed. If the energy-level structure of the unperturbed state is known, then the position (and sometimes shape) of the interfering state can be deduced.

A second consequence of predissociation is that the apparent lifetime of the fluorescence signal after excitation is shortened: the state may undergo a transition to the predissociative configuration before it can radiate. Contributions to the observed effective lifetime of an LIF signal, including predissociation, have already been highlighted above (Equation (7.4)). Predissociation occurs with probabilities reciprocally equivalent to time-scales of a few nanoseconds to a few picoseconds. Thus, from the measurement of the effective lifetime as a function of excited energy level, one will not only be able to deduce the energetic position of the predissociative potential, but also to extract information about the coupling strength (the quantum mechanical interaction matrix element). Principally, there are two ways to measure the temporal effect that predissociation has on an LIF signal. First, since the change in lifetime is associated with a change in line width (remember $\Delta\nu \approx \tau^{-1}$), one could try to measure the actual width of the transition lines. In general, this is not always possible, specifically if the excitation laser is a pulsed laser whose line width might be of comparable order, and/or if the spectral resolution of the detection system is insufficient to recognize (often subtle) differences in width. Second, the lifetime can be measured directly,

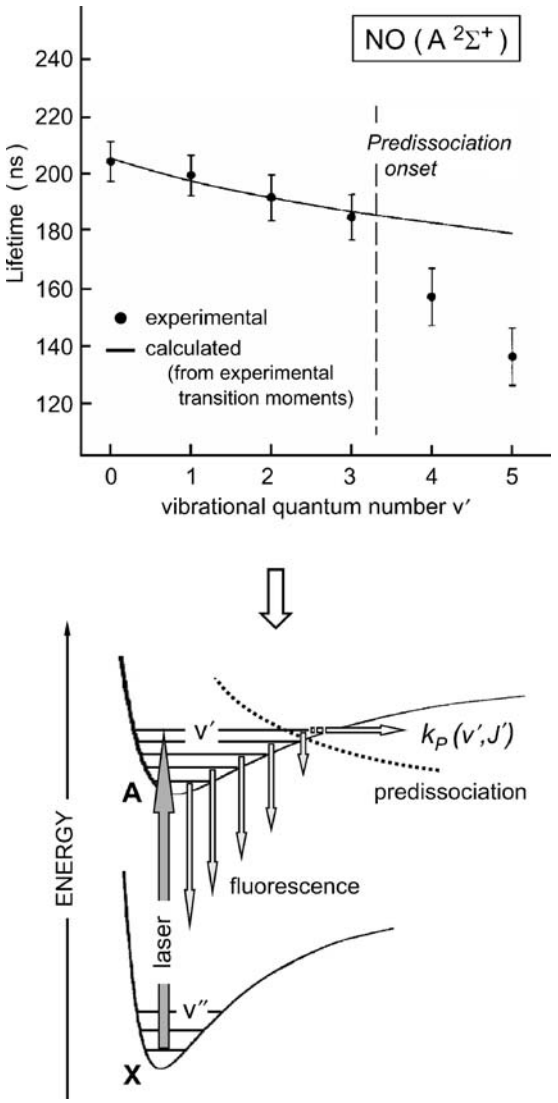

Figure 7.14 Comparison between experimental vibrational collision-free lifetimes and calculated radiative lifetimes for NO($A^2\Sigma^+$, $v' = 0-5$). Information about the crossing with the predissociative potential E_{cross} and the coupling strength $k_P(v', J')$ can be extracted from the data. Experimental data adapted from Luque and Crosley; *J. Chem. Phys.*, 2000, **112:** 9411, with permission of the American Institute of Physics

and provided that all other parameters affecting τ_{eff} are known one can extract the desired information on the predissociation process. An example of this approach is shown in Figure 7.14 for NO whose A state becomes affected by predissociation around its vibrational levels $v' \approx 3$–5.

Table 7.1 Summary of results from LIF experiments on NO ($A^2\Sigma^+$, $v' = 0-5$), including measured (collision-free) lifetimes, calculated radiative lifetimes, predissociation rates, and self-quenching constants. Data from Luque and Crosley (2000)

v'	τ_{exp} (ns)	τ_{rad} (ns)	$k_D(10^6\ s^{-1})$	$k_q(10^{-10}\ cm^3\ s^{-1})$
0	205 ± 7	206	–	2.8
1	200 ± 8	198	–	2.9
2	192 ± 8	192	–	2.6
3	184 ± 8	187	–	2.9
4	157 ± 8	183	0.9	7.1
5	136 ± 8	179	1.8	7.1

Figure 7.14 clearly reveals the deviation from the expected, calculated radiative lifetime beyond $v' = 3$. Using these calculated unperturbed values for τ, the predissociation rate constants can be extracted from the measured radiative lifetime values (see Table 7.1 for a summary), and these in turn can be used to deduce information about the quantum-mechanical coupling matrix elements.

7.3 Practical implementation of laser-induced fluorescence spectroscopy

There are probably as many different realizations of experimental LIF set-ups as there are research groups, with appropriate adaptations to any conceivable chemical reaction system, and more. The actual instrumental combinations depend on the complexity of the problem under investigation; in addition, financial constraints may play a significant role in the decision-making process (an experiment meant for an undergraduate teaching laboratory will most likely make use of much simpler and more basic components than those addressing front-line research issues, e.g. see Sikora *et al*, 1997). However, whatever the actual scientific problem, apparatus for LIF experiments follows the general design concepts depicted in Figure 7.15.

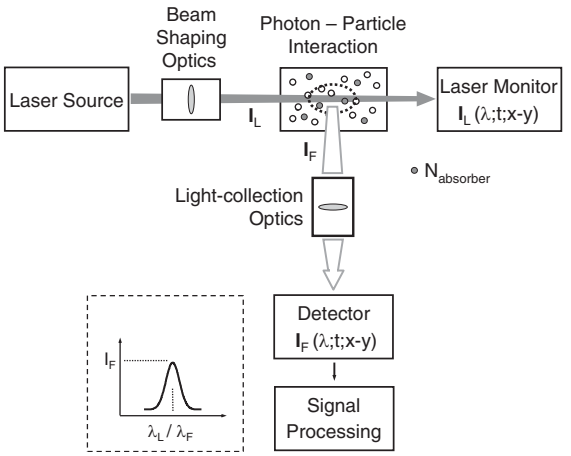

Figure 7.15 Generalized schematic of an experimental set-up for LIF spectroscopy

The main building blocks of any LIF set-up incorporate (i) the laser system, (ii) the reaction environment, and (iii) the fluorescence detection system. In addition, various ancillary groups might be encountered, such as optical components to shape the incoming laser beam, and most likely some imaging optics for efficient collection of the fluorescence emission. Also, some laser monitoring equipment is likely, measuring the laser's power, and temporal, spectral and spatial profiles.

A brief summary follows of all building blocks and the variety of components required for investigating particular aspects of a specific chemical reaction problem.

Nearly all types of laser system, mostly tuneable, have been used at one time or other, ranging from single-mode or narrow-bandwidth CW lasers (e.g. dye or semiconductor diode lasers), through standard pulsed lasers providing nanosecond pulses (e.g. dye or Ti:sapphire lasers), to ultra-short laser pulses with picosecond or femtosecond duration (e.g. mode-locked/CPM dye and solid-state lasers). The choice of laser is influenced either by the wavelength range or by the time regime of the molecular system under investigation, or both.

In principle, the photon–particle interaction environment can be of any shape and encompass any media parameter, depending on the chemical system under study. The interaction region can consist of a vacuum chamber, if particle beam experiments are conducted or if single collision conditions are desired. It can comprise a cell, in which the pressures of a reagent and buffer gases can be as low as a fraction of a millibar or as high as a few bar. Or it may simply be the ambient environment (e.g. for the investigation of atmospheric chemical reactions or the detection of trace molecules). Specific cases, which constitute aspects of the latter two, are burner flames and gas discharge tubes.

The beam-shaping optics for the laser beam often comprise a single lens, normally to focus the laser beam into the interaction region (1D excitation). Or the laser radiation is shaped like a plane sheet to realize multi-dimensional mapping of the interaction region (two-dimensional (2D) excitation).

For the monitoring of the laser radiation, a variety of instrumentation is used. Power or pulse energy meters monitor the photon flux through the interaction region; wave meters determine the exact (absolute) operating wavelength of the system, and Fabry-Perot interferometers provide (relative) scaling during a wavelength scan; time-sensitive photodiodes are used to record the temporal profile of laser pulses; and beam profilers determine the spatial intensity distribution across the laser beam.

For the collection of the fluorescence light and its imaging onto the detector, optical components (usually lenses) are selected to optimize the efficiency. The choice of detector system depends critically on the answers one wishes to obtain from interrogating the chemical reaction. Simple single-element photodiodes or photomultipliers are used, as are 1D or 2D array detectors (e.g. charge-coupled device (CCD) or time-gated intensified units); wavelength selectivity also can be implemented with varied resolution (e.g. using band-pass filters or standard spectrographs).

Finally, the signals from the detector are processed by electronic instrumentation of varied complexity. The most commonly found units are simple voltage or current amplifiers (no time resolution), lock-in amplifiers (when using modulated CW excitation) or boxcar integrators (when using nanosecond-pulse excitation).

Clearly, it is well beyond the scope of this textbook to review all possible experimental implementations of LIF. Here, we only describe basic realizations, highlighting a few selected examples, to demonstrate the versatility of the technique of LIF. More detailed

examples can be found in the chapters discussing specific chemical reaction problems and in the chapter on applications.

One-dimensional excitation laser-induced fluorescence experiments

Probably the most utilized of experimental set-ups since the conception of LIF is that of a collimated or focused laser beam (from a pulsed or CW laser) passing through a region in which a chemical reaction (uni- or bi-molecular) is taking place. That region can be the interior of a simple vapour cell, a molecular beam, a beam–gas arrangement, or the configuration of crossed molecular beams, and the environment in that reaction region may realize collision-free or collision-dominated conditions for the LIF probe. A typical example for a crossed molecular beam LIF apparatus is shown in Figure 7.16.

The system comprises a vacuum chamber with a molecular beam source at one end. The particle beam of reagents and/or products is interrogated in an observation region (in which reactions may be initiated by a reagent gas), at right angles, by pulses from a tuneable laser source. The LIF emission is monitored perpendicular to the plane formed by the particle and laser beams.

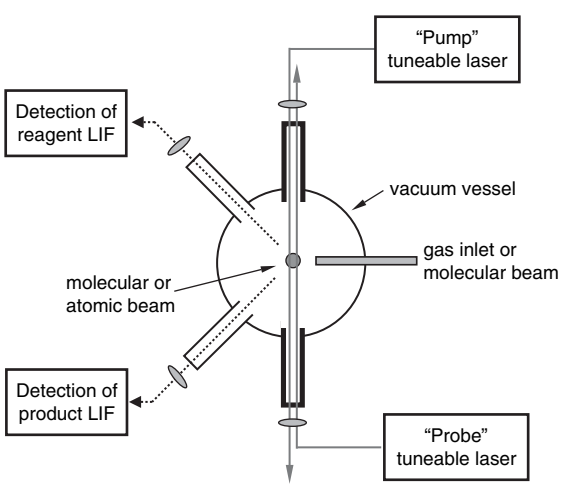

Figure 7.16 Typical beam–gas or crossed molecular beam apparatus, with one or two (pump/probe) tuneable lasers; LIF observation of both reagents and products is prepared, at 45° to the particle/laser beam axes

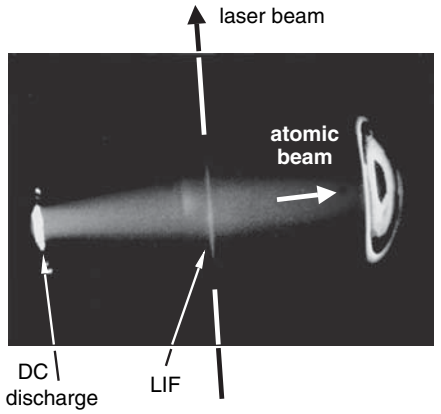

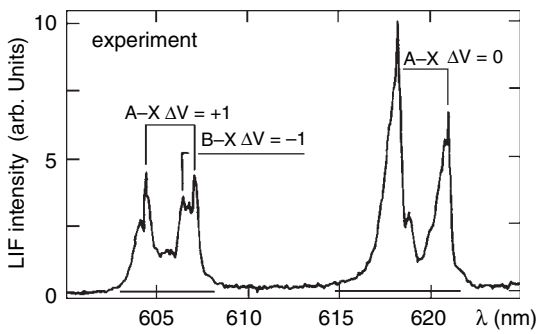

Figure 7.17 LIF spectroscopy of the beam–gas reaction $Ca(^3P)+HCl \rightarrow CaCl(X) + H$, revealing part of the rotational level population of the reaction product. Data adapted from Verdasco *et al*; *Laser Chem.*, 1990, **10:** 239, with permission of Taylor & Francis Group

An typical example of a beam–gas reaction is shown in Figure 7.17 for the reaction $Ca^*(^3P_J) + HCl \rightarrow CaCl(X; \nu'', J'') + H$. Note that the reaction with ground state $Ca(^1S_0)$ is endothermic; this is why excited Ca atoms are required, which are generated here in a discharge (laser excitation has also been realized). When interrogating the centre of the reaction cell with a tuneable CW laser, LIF emission is observed on transitions in the CaCl(A–X) band system. An example of a fraction of the related LIF excitation spectrum is shown in the lower part of Figure 7.17.

Closer inspection of the photograph of the interaction zone reveals that the narrow-bandwidth laser ($\Delta\nu_L \approx 10$ MHz) in fact interrogates sub-groups of the Doppler profile ($\Delta\nu_D \approx 50$ MHz). To the left of the main LIF emission needle, faint secondary

LIF is observed; this stems from reflection of the laser beam at the exit window of the vacuum chamber; the reflected beam probes a different velocity sub-group. The two LIF features counter-move when the laser is tuned across the Doppler profile.

Two-dimensional excitation laser-induced fluorescence experiments

Many modern photodetectors have a 2D CCD chip as their light-sensitive element. Such detectors constitute nothing else but a sensitive camera. Thus, it was only a logical step that this 2D capability was exploited in LIF measurements, in which spatial information about the reaction within the probe volume was desirable, but where scanning a collimated laser beam across the area would have been extremely time consuming. Furthermore, in situations of transient phenomena, insufficient time might be available to execute such a scan. The solution to the problem is simple: the laser beam is expanded in one spatial dimension (using a cylindrical lens) and focused in the dimension perpendicular to it (using a spherical lens). In this way, a sheet of laser radiation is generated. This implementation of LIF is now commonly known as planar-LIF (PLIF). The principle is shown schematically in Figure 7.18.

Very common applications for PLIF are found in the study of combustion (e.g. flames of burners and combustion engines), but other areas, like the visualization of explosive shockwaves and the imaging of stereodynamics of single-collision chemical reactions, to name but a few, are also popular applications for PLIF. An example is shown in Figure 7.19 for the analysis of the flame of a standard methane–air burner (e.g. see Bombach and Käppeli (1999)). It further highlights the versatility of the technique for 2D simultaneous visualization of multiple radicals generated in the burning process.

In the particular case shown here, the excitation wavelengths for the radicals CH_2O, CN and CH (amongst many others) are realized by a single tuneable laser source (wave frequency ω_1), and non-linear conversion of its fundamental wavelength (frequency doubling $2\omega_1$ and mixing $\omega_1 + \omega_2$). By selecting the wavelength of the laser source carefully, two species can be excited simultaneously, as indicated in the excitation spectra. When imaging the flame, the predominance of particular radicals in certain regions of the flame reflects the different temperature conditions in the combustion volume.

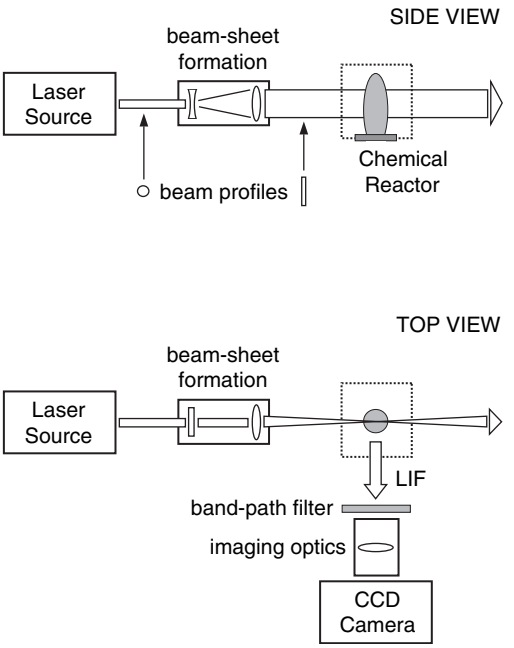

Figure 7.18 Typical experimental set-up for PLIF

Time-resolved pump–probe laser-induced fluorescence experiments

A frequently used variant of standard LIF set-ups is the addition of a second, independent (tuneable) laser source. The second laser promotes the molecule from the level of the first excitation to a higher energy state. The principle is shown schematically in Figure 7.20.

In the early days of this type of two-step excitation, also known as optical–optical double resonance (OODR), one major aim was to be able to access molecular states (electronic states and vibrational levels) that were not normally accessible via single-photon excitation. However, it was soon realized that the temporal independence of the two lasers would easily allow for the probing of dynamics in the system. Although this approach had only limited applicability (only dynamical processes of the order

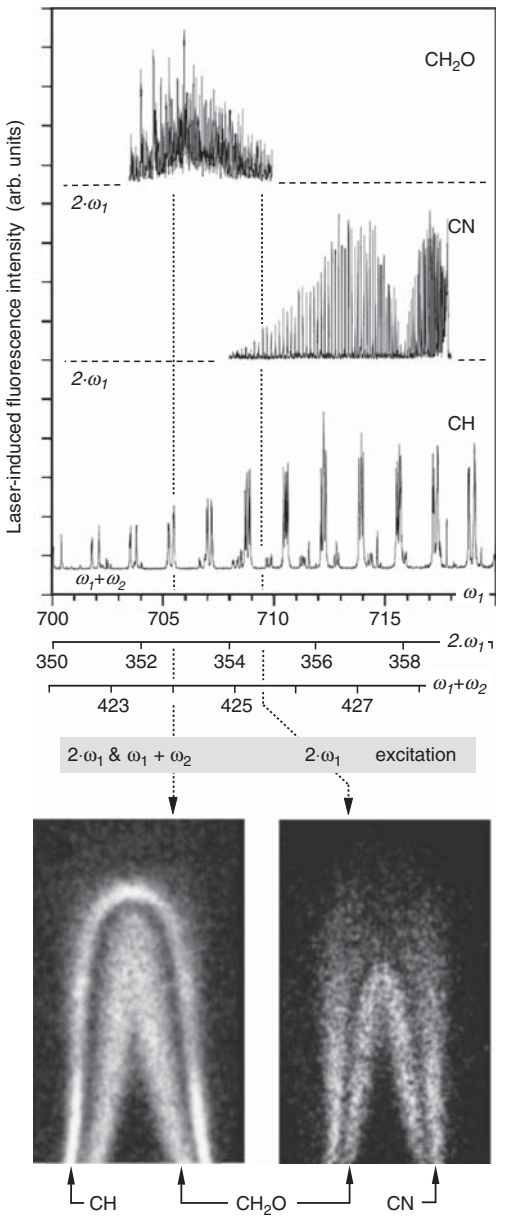

Figure 7.19 Simultaneous LIF excitation spectra of the reaction radicals CH_2O, CN, and CH in a methane–air burner flame. Wavelength scales: ω_1 is the fundamental wave of dye laser; $2\omega_1$ is the second harmonic wave; $\omega_1 + \omega_2$ is the sum frequency wave of dye laser plus fundamental wave of Nd:YAG laser (all in units of nanometres). The PLIF images reveal the predominance of various reaction radicals in different parts of the flame. Data adapted from Bombach and B. Käppeli; *Appl. Phys. B*, 1999, **68**: 251, with permission of Springer Science and Business Media

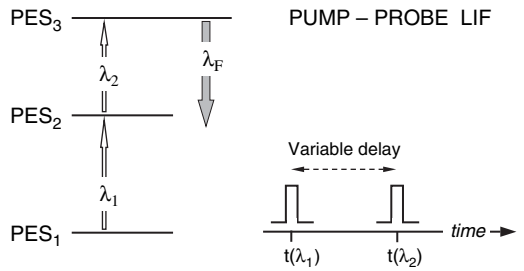

Figure 7.20 Principle of pump–probe LIF using pulsed lasers; the probe laser pulse (at λ_1) is delayed with respect to the pump laser pulse (at λ_2)

of or longer than the widely available standard nanosecond laser pulses could be studied), the advent of ultra-short pulse laser sources some 20 years ago changed things dramatically. Now, 'real' chemical process dynamics could be followed: femtochemistry was born; and one of its pioneers, Ahmed Zewail, received the 1999 Nobel Prize for Chemistry for his contributions to the study of chemical processes on the femtosecond scale.

The pioneering experiment carried out in Zewail's group is the probing of the photo-fragmentation of ICN into its products I + CN (Rosker *et al.*, 1988). A first femtosecond laser pulse promotes ICN from its ground state into a transition state (a repulsive PES). Once in this state the molecule immediately dissociates on the time-scale of less than 1 ps (a value typical for the many intra- and inter-molecular dynamic processes). Using a second femtosecond laser pulse, the excitation to a higher lying (equally dissociative) PES results in the generation of fluorescence emission on the CN(B–X) band. Tuning the laser to wavelengths associated with the resonance energy between the two excited PESs at distinct internuclear configurations, and then scanning the relative time delay between the two femtosecond laser pulses, results in probing of the dynamics of the dissociation. The ICN experiment is described in more detail in Section 19.1. Other examples of this exciting field of research will be discussed in Parts 4–6.

To conclude the section on LIF techniques, we describe a 2D chemical process probing exploiting a PLIF set-up, in which time evolution of a chemical process is resolved. Such a set-up is appropriate in situations in which one not only wishes to follow the

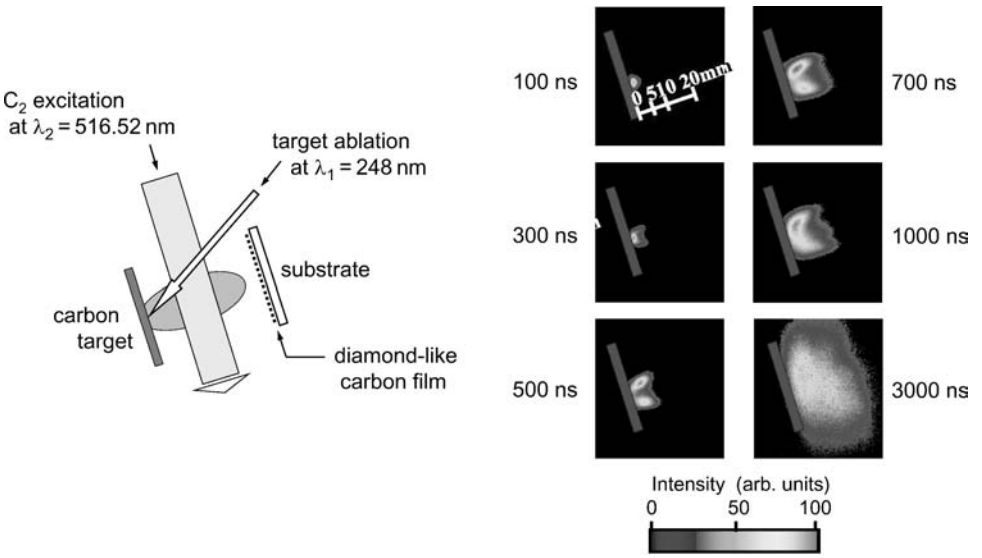

Figure 7.21 LIF emission images from C_2-molecules, generated by laser ablation of a solid carbon target and probed by time-delayed laser pulse on a Swan-band transition. Data adapted from Yamagata *et al*; *Mat. Res. Soc. Symp.*, 2000, **617:** J3.4, with permission of the Material Research Society

temporal evolution of a chemical process, but also wants to record its spatial evolution linked to time. One illustrative example is shown in Figure 7.21 for the practical problem of monitoring the evolution of a laser-generated plasma typically used in thin-film vapour deposition. The particular case here is that of diamond-type carbon deposition (e.g. Yamagata *et al*., 2000).

The plasma component followed here is the dimer C_2, with excitation (delayed with respect to the laser pulse initiating carbon ablation) on the (0, 0) transition and LIF emission on the (0, 1) transition within the Swan-band $a^3\prod_u - d^3\prod_g$. Clearly, the evolution in space and time can be traced in the snapshots of the plasma volume, with the distribution of C_2 becoming more homogeneous with time.